The magma-hydrothermal transition zone on the East Pacific Rise

Gen Ito

Introduction

Deep beneath the ocean surface where no sunlight can reach, a world filled with strange creatures exists. Tube worms, enormous mussels, shrimps, and other eye-opening views are encountered at hydrothermal vent sites. Metal-rich fluids flowing from hydrothermal vents support the life found here. Hydrothermal vents are characterized by hot fluids rising from chimneys made of mineral deposits that precipitate out of the fluids (Figure 1). Hydrothermal vent field sites are mostly distributed along sea floor spreading centers. Not only because they posses astonishing biological communities, hydrothermal systems have been a widely discussed topic in Earth science because of their geological importance.

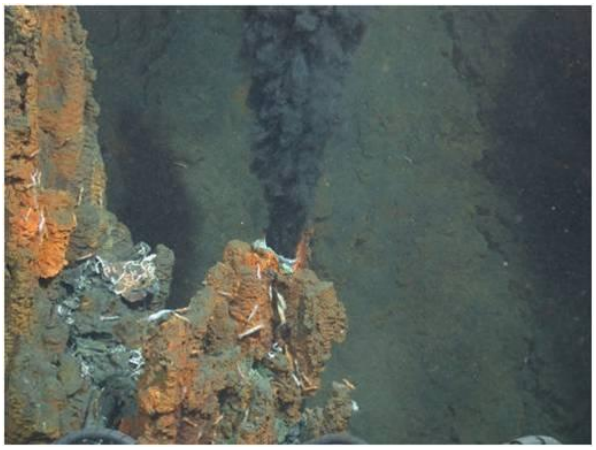

Figure 1. A sample image of a black smoker. Hydrothermal fluid is coming out from the vent. Photograph courtesy of William Seyfried, University of Minnesota, Twin Cities.

In terms of Earth's energy, hydrothermal systems remove approximately 30% of the heat lost from oceanic crust (Sclater et al., 1981; Stein and Stein 1994). In terms of materials, seawater chemical and isotopic compositions are affected by fluids flowing out from these vents (Edmond et al., 1979a; Thompson, 1983). Additionally, crustal composition is altered, creating heterogeneities in the mantle when this crust is subducted (Zinder and Hart, 1986) and further

affecting compositions of volcanic rocks in island arcs (Perfit et al., 1980; Tatsumi, 1989). Considering this wide range of geological influences of hydrothermal systems, it is of great interest to study them in detail.

The most direct way to study these hydrothermal systems is to focus on the vents and fluids coming out of these vents on the ocean floor surface. Even though hydrothermal vent field sites are located beneath kilometers of seawater, they can be directly accessed with submersibles and submarines. For aqueous geochemistry, this approach is very effective as it allows direct observations and samplings by expert scientists in real time. However, what is apparent on the surface for these hydrothermal systems does not paint the whole picture. Crucial chemical reactions take place in the subsurface where fluids cycle through hot and pressurized rocks. It is not easy to study the subsurface because of technical reasons such as the necessity to drill through crystalline bedrock under a few kilometers of water. When studying the subsurface, the technical obstacles can be avoided by building theoretical models or experimental models in a laboratory setting. Another approach is to study the past hydrothermal vent field sites. On land, ophiolites, fragments of uplifted oceanic crust (Moores and Vine, 1971; Coleman, 1977; Casey et al., 1981; Harper, 1984; Nicolas, 1989), can provide valuable information without going undersea. Tracers of hydrothermal systems are preserved in the geological record in ophiolites. Nevertheless, direct drilling of in situ oceanic crust can provide insights not available from ophiolites and remains an important task in marine geology. The Integrated Ocean Drilling Program (IODP) is responsible for marine drilling aimed for scientific purposes. On the ocean floor, rocks in inactive, fossil hydrothermal field sites are easier to drill than active ones because there are fewer fractures, and sediment deposits on top of crystalline bedrocks aid the drilling process. Four IODP expeditions created Hole 1256D, which extends down to the base of sheeted

dikes, and the last expedition, Expedition 335, collected samples from the dike-gabbro transition zone. This paper investigates the hydrothermal alteration of this transition zone through geochemical analysis of secondary minerals.

Geological setting

Hole 1256D is located at 6.736° N, 91.934° W (Wilson et al., 2006) on the Cocos Plate in the eastern Pacific Ocean (Figure 2). The oceanic crust here was created at the East Pacific Rise

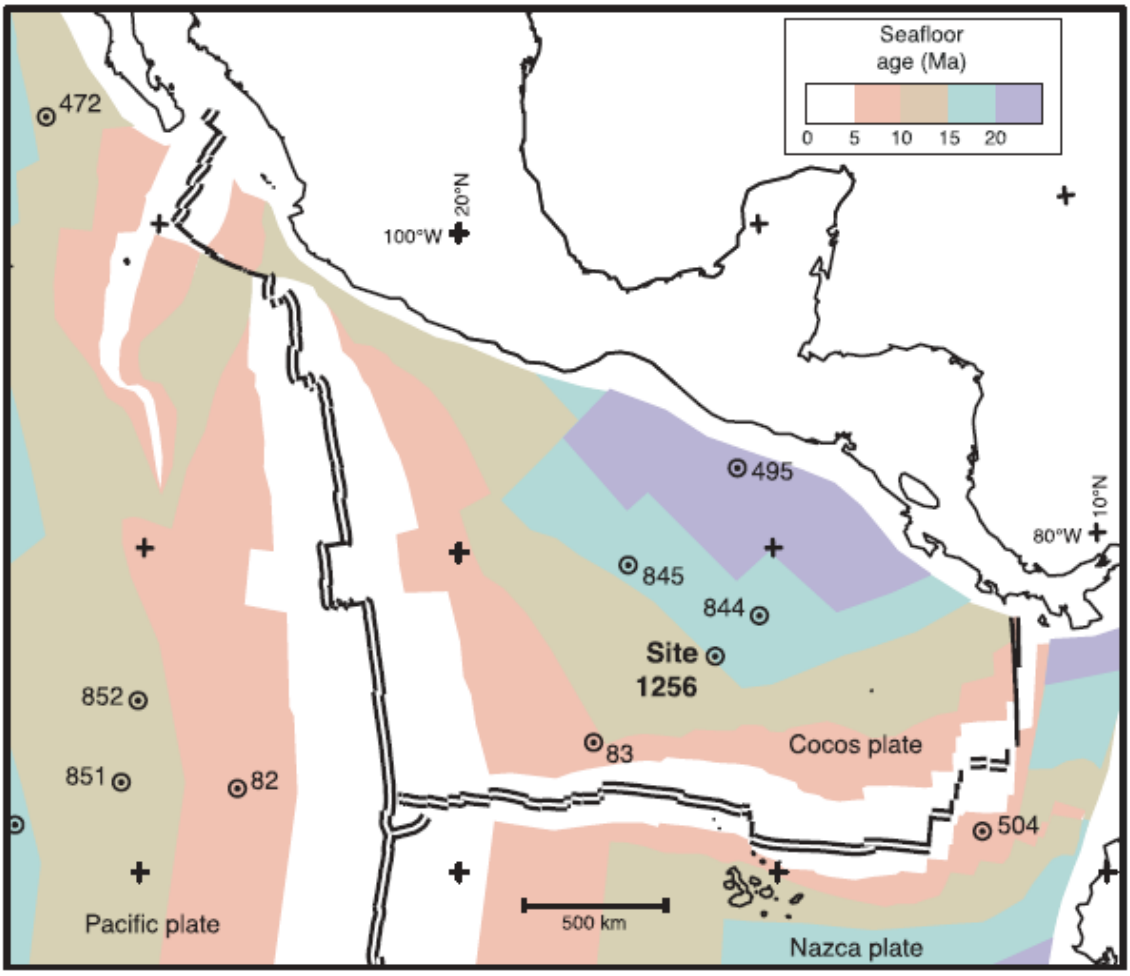

Figure 2. Location of Site 1256, located in the Pacific Ocean off the coast of Central America. Color grading indicates the age of seafloor rocks (modified from Alt et al., 2010 and Wilson et al., 2003).

(EPR) approximately 15 million years ago (Ma) at a superfast spreading rate (Teagle and Expedition 309/312 Scientists, 2006; Wilson et al., 2006). A cross-sectional diagram of a typical spreading center at the EPR and the lithostratigraphy of Hole 1256D can be seen on Figures 3 and 4, respectively. The top portion of the oceanic crust is composed of basaltic volcanic flows; pillow basalts, massive flows, and breccias fill the upper kilometer (Alt et al., 2010). Under the volcanic flows is about 350 m thick sheeted dike complex that contains vertical sheet-like feeders (Teagle and Expedition 309/312 Scientists, 2006; Tominaga et al., 2009). Then, gabbroic rocks lie below the sheeted dike complex. These are coarse-grained rocks that formed by slowly-cooling magma (Alt, 1995). Typically, it is believed that a magma chamber is present within the gabbro from seismic studies. This magma chamber is less than a few hundred meters thick, 1-2 km wide (McClain et al., 1985; Detrick et al., 1987; Kent et al., 1990; Sinton and Detrick, 1992), and is referred to as a "melt lens". This is the heat source that drives hydrothermal circulation. Further below the melt lens is interpreted to be a crystal mush surrounded by hot rock from low seismic velocity data (Vera et al., 1990; Toomey et al., 1990; Harding et al., 1989; Sinton and Detrick, 1992).

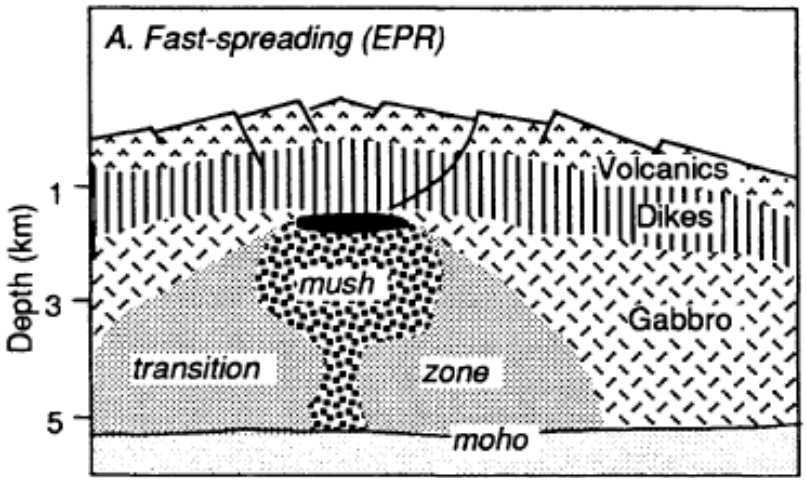

Figure 3. Cross-sectional view of a model of fast spreading center. Different rock layers and heat source can be observed. Melt-lens is located at the top of "mush" zone (modified from Alt, 1995 and Sinton and Deterick, 1992)

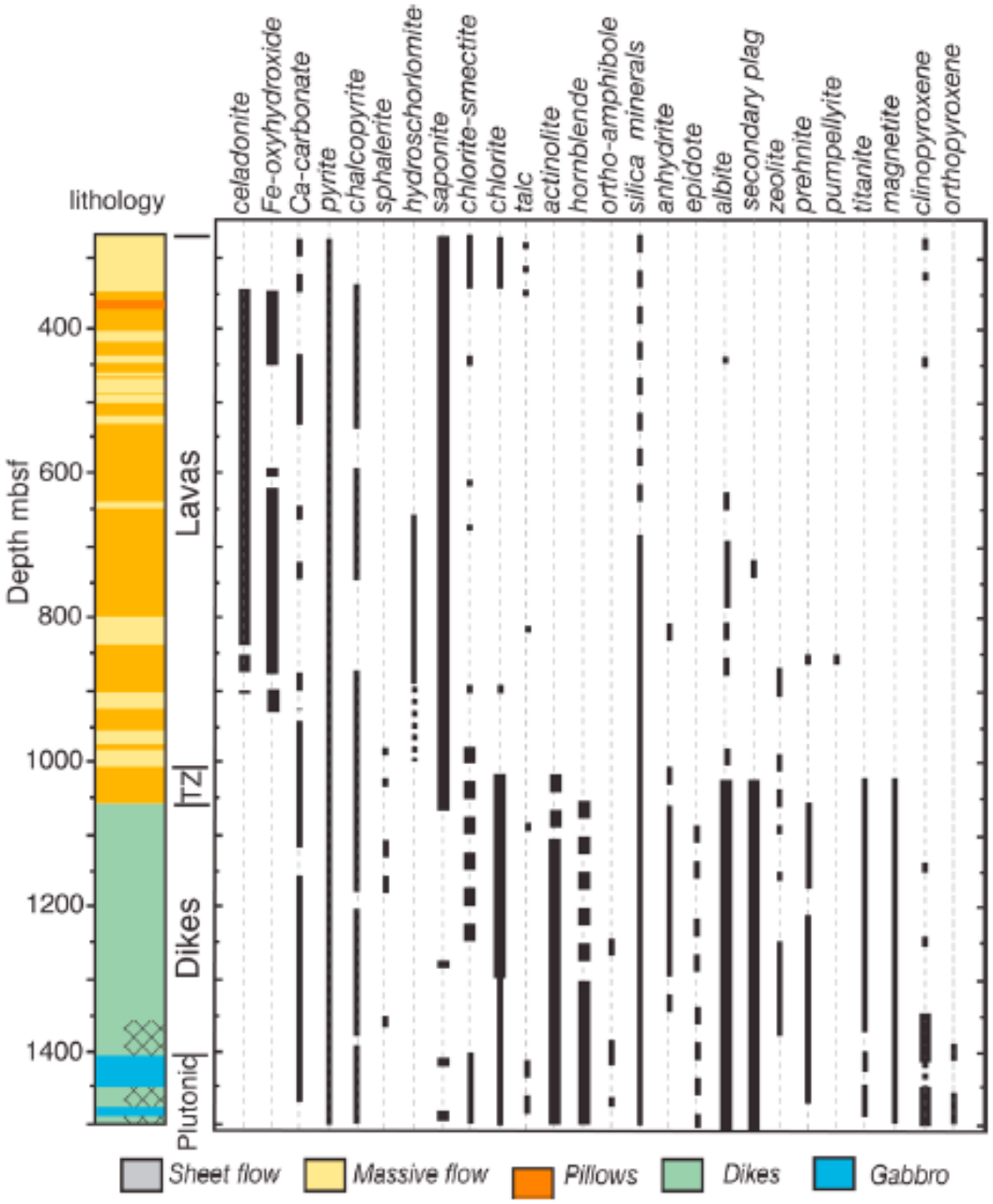

Figure 4. Lithostratigraphy at Hole 1256D. Distribution of secondary minerals is also shown (modified from Alt et al., 2010).

Fluid circulation

The composition of the subsurface is important because more porous and permeable sections allow easier circulation of fluids. Many fractures present in the volcanics make this

section the most porous and permeable (Alt, 1995). Considerably greater volumes of fluids circulate in the volcanic section compared to the sheeted dike complex or the gabbroic section. The lower part of the volcanic section has lower porosity and permeability than the upper portion because smectite and other secondary minerals fill in the fractures (Alt, 1995; Pezard, 1990).

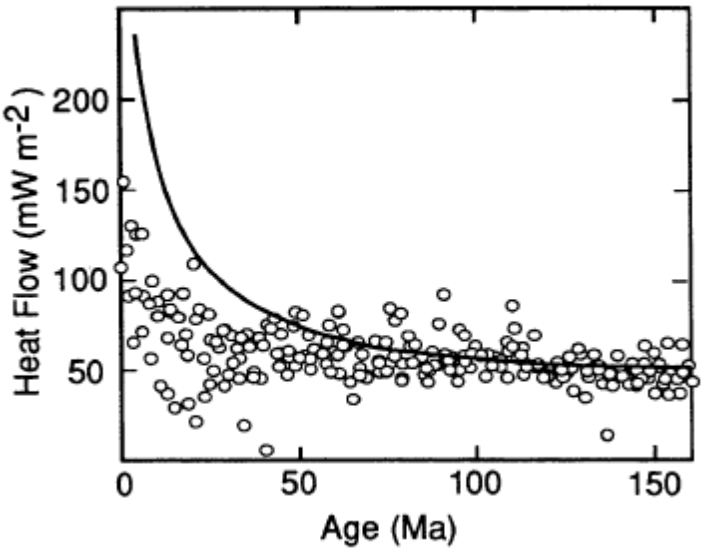

Figure 5. Relationship between oceanic heat flow and age of oceanic crust. Black curve is based on theoretical model and circles are actual, measured values. Measured values fall below the theoretical values, indicating the presence of other cooling mechanism. Convective cooling by circulating seawater is causing the actual heat flow values to be less than what is predicted from the theoretical heat flow model (modified from Alt, 1995 and Stein and Stein, 1994).

Heat flow studies have indicated theoretically that seawater is circulating through the subsurface of oceanic crust (Lister, 1972; Williams et al., 1974; Anderson and Hobart, 1976; Stein and Stein, 1994) (Figure 5). Most spectacular action occurs in the "active" system (Lister, 1982). Active system is an area directly above and relatively close to the melt lens or a heat source, and is best characterized by having focused discharge flows of high temperature fluids (Alt, 1995). On the seafloor surface, this focused flow creates black smokers and the well-known features of a hydrothermal vent field site. Away from the active zone is the passive zone. Convection in passive zones is slower and cooler than active zones because there is no melt lens nor a heat source but rather heat provided by the cooling of the lithosphere (Alt, 1995; Lister, 1982; Fehn et al., 1983). It is

estimated that passive convection accounts for 80-92 % of hydrothermal heat flux (Morton and Sleep, 1985; Stein and Stein, 1994; Mottl and Wheat, 1994).

Expeditions 309, 312, and 335

Named the "Superfast Spreading Rate Crust" mission, IODP expeditions 309, 312, and 335 tried to drill a complete section of the upper oceanic crust, through sediment, the upper lavas through dikes and into underlying gabbros. Expedition 309 resumed the work started by Ocean Drilling Program (ODP) Leg 206 to establish Hole 1256D. Expedition 309 drilled into the upper dikes and succeeded by Expedition 312 to drill down into granoblastic dike/gabbro

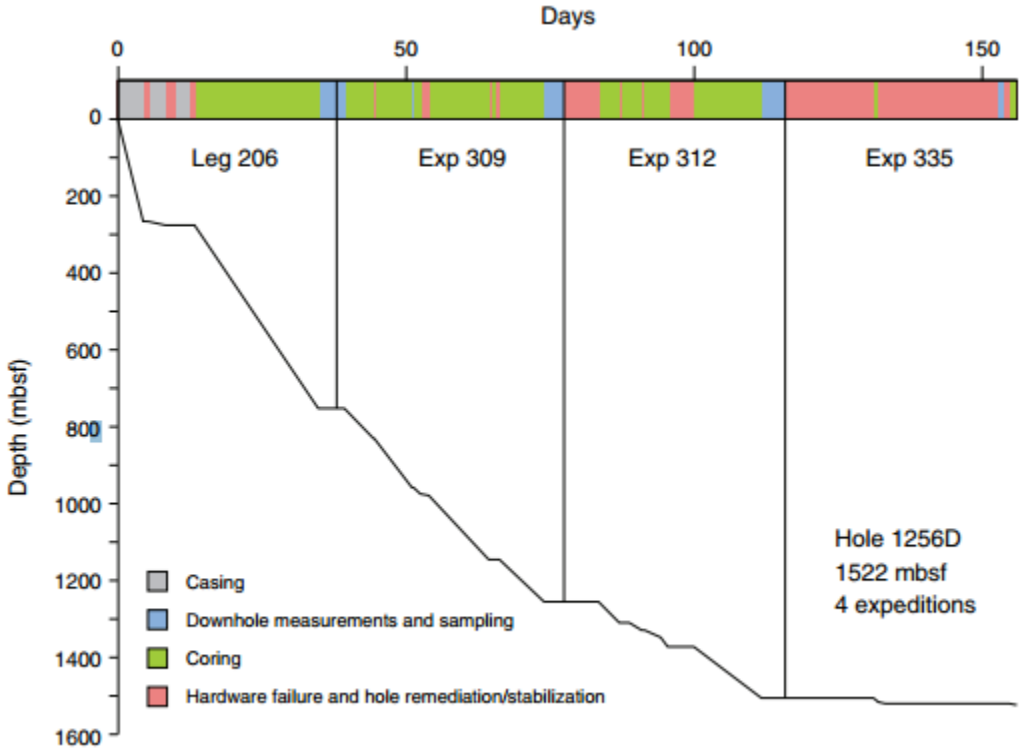

Figure 6. Drilling process of Hole 1256D over four scientific ocean drilling cruises with description of the activities taking place for each time period (modified from Expedition 335 Scientists, 2011).

transition zone. Expedition 335 did not penetrate much further, deepening the well to 1521.6 meters below sea floor (mbsf) from the initial depth of 1507.1 mbsf (Expedition 335 Scientists, 2011). The progress of each expedition is shown in Figure 6.

Nevertheless, partially to completely recrystallized glanoblastic basalt and gabbroic rock samples were recovered. Among these, crosscutting and overprinting hydrothermal alterations were observed (Expedition 335 Scientists, 2011). Expedition 335 Scientists (2011) believe that these granoblastic basalt and gabbros represent the upper crust – lower crust transition zone. Furthermore, they claim that the occurrence of amphibole in veins and patches indicate high hydrothermal fluid activities during formation. This study specifically investigates these rocks recovered from Expedition 335 at depths of approximately 1500 mbsf.

Hole 1256D

Hole 1256D was a very successful achievement; Koepke et al. (2011) says it is "the first complete penetration of the upper oceanic crust reaching the gabbroic section, and represents a unique reference section for the dike/gabbro transition in fast spreading ocean crust." Major studies (Wilson et al., 2006; Teagle et al., 2006; Koepke et al., 2008; France et al., 2009b; Alt et al., 2010; Koepke et al., 2011) that investigated the geochemistry and petrology of cores recovered from Hole 1256D devised two main models (Figure 7). Teagle et al. (2006), Wilson et al. (2006), Koepke et al. (2008), and Alt et al. (2010) follow the model in Figure 7a. According to this model, Hole 1256D penetrated into a contact-metamorphosed granoblastic dike section that contains gabbroic intrusions. It is believed that, in this model, Hole 1256D is about to reach the fossilized magma chamber; pyroxene equilibrium temperatures of 850-1050 °C (Koepke et al., 2008; Alt et al, 2010) indicated that granoblastic zones have a possibility of generating partial melts of trondhjemitic composition (Koepke et al, 2011). These studies are consistent with

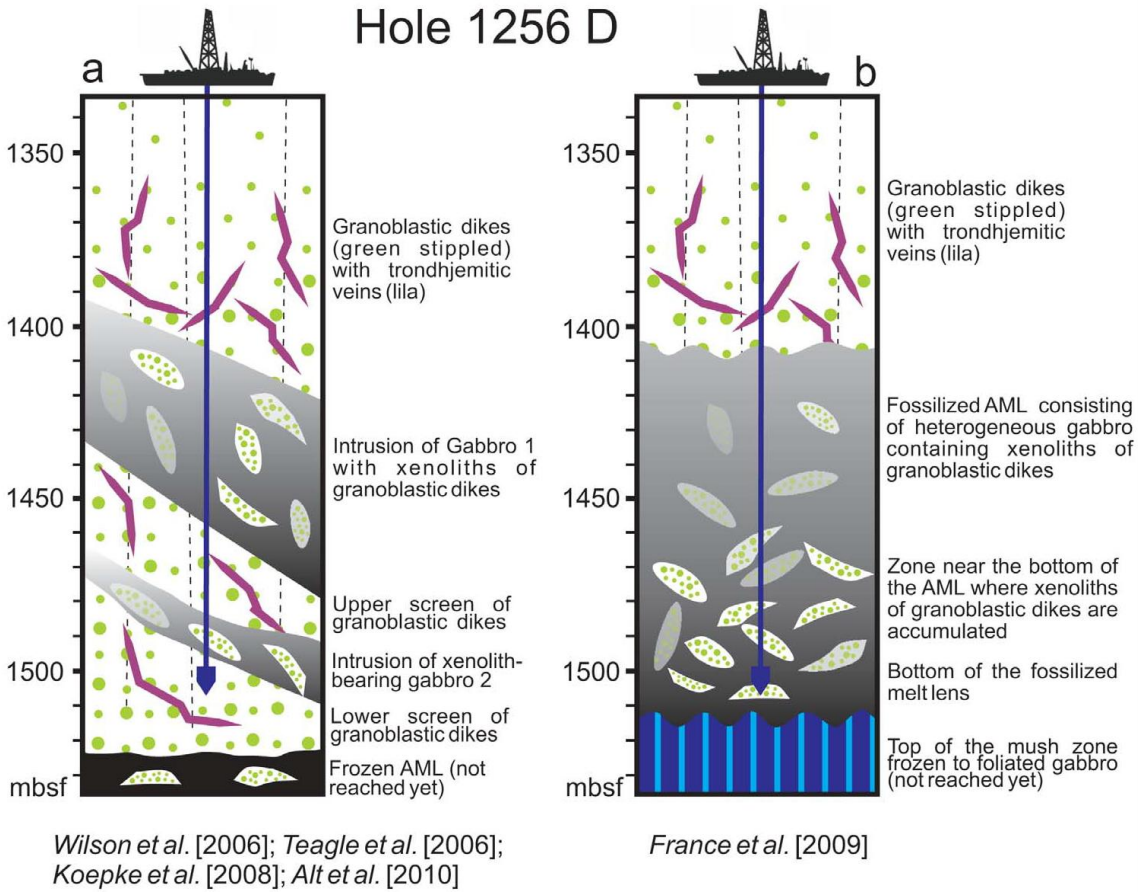

Figure 7. Diagram of dike/gabbro transition zone at Hole 1256D presented by Koepke et al., 2011. The same lithostratigraphy is interpreted in two different ways by different authors.

thermal metamorphism by a deep heat source (Koepke et al., 2011). On the other hand, France et al., 2009b suggest a different approach for the same data used in other studies. This work interprets the entire section beneath about 1400 mbsf as one, continuous gabbro with xenoliths of granoblastic dikes almost "floating" inside (Figure 7b). This gabbro is thought to be the fossilized axial melt lens. Here, a frozen "mush" zone is expected to be present deeper in the crust. In order to make conclusions to which model better illustrates Hole 1256D and hydrothermally altered oceanic crusts in general, deeper drilling is necessary. A few hundred meters more of core recovery can provide data to answer many of the current uncertainties. However, until this happens, more research must be done for the purposes of both advancing

knowledge and motivating future ocean drilling projects. This study tries to accomplish this by mainly classifying the minerals based on their chemical composition and determining the temperatures at the time of formation from the core recovered at Hole 1256D.

Methods

Thin sections of the samples were prepared and analyzed at the University of Michigan using a Cameca SX – 100 Electron Microprobe Analyzer. Before the analysis, thin sections were carbon coated to avoid charge build-up during analysis. The Cameca SX – 100 Electron Microprobe Analyzer has four wavelengths dispersive spectrometers. A 15 kV accelerating voltage, 15 nA specimen current, and 10 second counting times were used for this analysis. Si, Al, Ti, Fe^{2+}, Mn, Mg, Ca, Na, K, and Cl were analyzed and reported as wt. % oxides. Minerals were classified according to the chemical composition from these microprobe analyses.

The temperatures of mineral formation were calculated using the edenite-richterite (with or without quartz) thermometer from Holland and Blundy (1994). By analyzing the composition of amphiboles and plagioclase that are located next to each other, temperature of the mineral at the time of crystallization can be calculated. The underlying theory here is related to diffusion. Stemming from the basic solid solution concepts in amphiboles, $Mg^{M2}Si^{T1} \leftrightarrow A1^{M2}A1^{T1}$ and $Na^{M4}A1^{M2} \leftrightarrow Ca^{M4}Mg^{M2}$, the authors develop a calculation procedure for amphiboles based on more complex models. For plagioclase, they follow DQF (Darken's Quadratic Formalism) model given in Holland and Powell (1992). According to the authors, "the thermometer takes into account non-ideal mixing in both amphibole and plagioclase and is calibrated against an extensive dataset of natural and synthetic amphiboles". Therefore, thermometry presented by Holland and Blundy (1994) is relevant to this study. Edenite-richterite thermometer has the following formula:

$$T = \frac{78.44 + Y_{ab-an} - 33.6X_{Na}^{M4} - (66.8 - 2.92P) \cdot X_{Al}^{M2} + 78.5X_{Al}^{T1} + 9.4X_{Na}^{A}}{0.0721 - R \cdot \ln\left(\frac{27 \cdot X_{Na}^{M4} \cdot X_{Si}^{T1} \cdot X_{an}^{plag}}{64 \cdot X_{Ca}^{M4} \cdot X_{Al}^{T1} \cdot X_{ab}^{plag}}\right)}$$

T is temperature in kelvins, P is pressure in kbar, and R is the universal gas constant 0.0083144 kJ K^{-1} mol^{-1}. Each of the amphibole X terms represents specific sites of a cation within amphibole where the sites are shown in superscripts. Site allocation in amphiboles is dependent on coordination number and charge of an ion. "T" stands for tetrahedral site, and it usually houses silicon ions and sometimes aluminum ions. M4 sites are 6- to 8- coordinated, accommodating larger cations such as Na and Ca. M2 sites are smaller and are strictly in octahedral coordination. Here, cations of aluminum, iron, and magnesium usually get incorporated. The A site is the largest site, which has 10- to 12- coordination. Large cations like sodium, and even potassium, can be incorporated into the A site. There are other sites in the amphibole structure, including T2, M1, and M3, but only T1, M2, M4, and A sites are necessary for the thermometer presented by Holland and Blundy (1994). Calculations of these amphibole X terms are shown below where all cations are in molar quantities obtained from mineral formulae.

$X_{Si}^{T1} = (Si - 4)/4$ $\qquad$ $X_{Na}^{A} = Ca + Na + cm - 2$

$X_{Al}^{T1} = (8 - Si)/4$ $\qquad$ $X_{Na}^{M4} = (2 - Ca - cm)/2$

$X_{Al}^{M2} = (Al + Si - 8)/2$ $\qquad$ $X_{Ca}^{M4} = Ca/2$

cm stands for "cummingtonite" substitution which can be obtained by the formula

$$cm = Si + Al + Ti + Fe^{3+} + Fe^{2+} + Mg + Mn - 13.0$$

X_{an}^{plag} and X_{ab}^{plag} are percentages of Ca and Na in plagioclase, respectively. Calculation formulae are:

$X_{an}^{plag} = Ca/(Ca + Na)$ $\qquad$ $X_{ab}^{plag} = Na/(Ca + Na)$

Y_{ab-an} is dependent on the composition of plagioclase; if X_{ab} is greater than 0.5,

$$Y_{ab-an} = 3.0\ kJ$$

Otherwise,

$$Y_{ab-an} = 12.0(2X_{ab} - 1) + 3.0\ kJ$$

In order to use the edenite-richterite thermometer and terms associated with it, the atomic composition of amphiboles must be recalculated from the original composition obtained using microprobe analysis. The amount of ferric iron in an amphibole is a key factor in its chemical composition. Ferric iron contents are too low to use the thermometer if any one of the following holds true.

1. $\Sigma > 16$ $\quad f_1 = 16/\Sigma$
2. $Si > 8$ $\quad f_2 = 8/Si$
3. $(\Sigma - Na + K) > 15$ $\quad f_3 = 15/(\Sigma - Na - K)$
4. $Ca > 2$ $\quad f_4 = 2/Ca$
5. All iron are ferrous $\quad f_5 = 1.00$

Σ is the sum of all cations (Si, Al, Ti, Fe^{2+}, Mn, Mg, Ca, Na, K, and Cl). *f* terms are factors that are used to recalculate amphibole chemical formulae. On the other hand, too much ferric iron is present if:

6. $(Si + \text{total Al}) < 8$ $\quad f_6 = 8/(Si + Al_{total})$
7. $(\Sigma - K) < 15$ $\quad f_7 = 15/(\Sigma - K)$
8. $(\Sigma - Na - K - Ca) < 12.9$ $\quad f_8 = 12.9/(\Sigma - Na - K - Ca)$
9. $Fe^{3+} > (2 - Al^{vi} - Ti)$ $\quad f_9 = 36/(46 + Al_{total} + Si + Ti)$
10. All iron are ferric $\quad f_{10} = 1 - (Fe_{total}/46)$

1 through 5 are the upper bound and 6 through 10 are the lower bound factors. Then, the minimum *f* from 1 ~ 5 (f_A) and maximum *f* from 6 ~ 10 (f_B) are chosen to obtain f_{av}, the average of the two values. During this process, f_B must be greater than f_A and less than 1.00 for the analysis to succeed. Additionally, if any f_A value is less than 1.00, it is set to 1.00. Once f_{av} is obtained, each of the cations is multiplied by f_{av} to renormalize amphibole composition. Finally, amounts of ferric and ferrous iron are determined by:

$$Fe^{2+} = Fe_{total} - Fe^{3+} \qquad Fe^{3+} = 46(1 - f_{av})$$

From the recalculated values of each cation, the chemical formulae of the amphiboles are determined and consequently provide values necessary to calculate the temperature using the edenite-richterite thermometer.

Results

The microprobe analysis results are shown in Table 1. Each element is reported in wt. % oxides. According to the chemical composition, minerals were identified and labeled. A well run analysis of amphiboles has a total less than 100%, usually yielding 98%. This is due to the hydrous component of amphiboles that are not detectable by the instrument because of the low atomic number of oxygen and hydrogen atoms. The identification of amphiboles mainly focused on aluminum and alkali (mostly Na) elements after selecting samples with a total close to 98%. Compared to plagioclase, amphiboles have considerably less aluminum and alkali elements but are enriched in iron and magnesium. On the other hand, plagioclase has significant amounts of aluminum, frequently around 20%-25%. The total for plagioclase yields approximately 100%. Also, plagioclase has higher silica content than amphiboles. Based on these, amphibole and plagioclase, the two minerals necessary for temperature calculation, were confirmed.

Chlorite is the third major mineral analyzed in this study. The oxide total for chlorites yields ~80% to ~90%. As with amphibole, chlorites have a hydrous component in their chemical structure, and in fact they are more hydrous than amphiboles. This makes the total for chlorites significantly less than plagioclase or amphiboles. Additionally, chlorites contain abundant iron, magnesium, and aluminum in comparison to silicon which can frequently be less than 30%. Epidote is another mineral with a total significantly less than 100%. Like chlorite, it yields a total of approximately 90%, but the difference is that epidote contains much more calcium. Epidote can have 20% or more calcium oxides whereas chlorite only contains a few percent.

Table 1. Electron microprobe analysis of minerals. Each element is reported in wt. % oxides. For iron, Fe^{2+} is shown here. The first column indicates the sample number and the second column specifies the particular area within the sample. The last column is the identification of the mineral based on chemical composition. Mineral name abbreviations are as follows: amp: amphibole, chl: chlorite, ep: epidote, mt: magnetite, phl: phlogopite, plag: plagioclase, zeo: zeolite.

Sample	Point	SiO_2	Al_2O_3	TiO_2	FeO	MnO	MgO	CaO	Na_2O	K_2O	Cl	Total	Min
2pd_12	1	53.34	3.24	0.52	10.15	0.14	18.72	10.96	1.18	0.04	0.06	98.35	amp
2pd_12	2	53.19	2.07	0.71	10.17	0.09	18.36	11.31	1.21	0.05	0.07	97.23	amp
2pd_12	3	64.65	21.95	0.04	0.33	0.01	0.01	4.19	9.13	0.10	0.00	100.43	plag
2pd_12	4	52.61	1.50	0.83	10.45	0.08	18.29	11.30	1.27	0.05	0.06	96.42	amp
2pd_12	5	53.67	0.00	0.05	7.43	0.14	15.06	22.74	0.49	0.00	0.00	99.57	amp
2pd_12	6	54.37	1.30	0.48	10.82	0.15	18.61	11.29	0.91	0.02	0.06	98.02	amp
2pd_12	7	52.94	2.14	0.16	14.81	0.08	15.19	11.60	0.44	0.05	0.06	97.47	amp
2pd_12	8	53.69	0.00	0.06	7.38	0.16	15.14	22.60	0.50	0.00	0.00	99.51	amp
2pd_12	9	63.08	23.30	0.04	0.46	0.02	0.00	5.29	8.74	0.06	0.01	101.01	plag
2pd_12	10	52.32	2.34	0.29	14.64	0.06	14.67	11.75	0.43	0.09	0.10	96.69	amp
2pd_12_1	1	52.77	0.00	0.10	8.72	0.19	14.67	22.06	0.34	0.00	0.00	98.85	amp
2pd_12_1	2	51.89	2.70	0.16	18.54	0.30	12.60	11.90	0.23	0.01	0.01	98.35	amp
2pd_12_1b	1	57.56	0.98	0.11	14.81	0.05	21.39	0.16	0.26	0.04	0.01	95.38	amp
2pd_12_1b	2	52.27	1.75	0.13	18.36	0.33	12.33	11.62	0.20	0.01	0.01	96.99	amp
2pd_12_1b	3	32.50	13.02	0.00	23.92	0.09	16.25	1.31	0.04	0.05	0.01	87.20	chl
2pd_12_1c	1	57.19	0.50	0.09	13.77	0.05	22.30	0.28	0.21	0.02	0.00	94.42	amp
2pd_12_2b	1	0.00	0.09	47.68	42.91	3.87	0.10	0.04	0.00	0.00	0.00	94.71	mt

2pd_12_2b	2	50.79	3.12	0.80	10.08	0.14	18.57	10.70	2.22	0.09	0.61	97.24	amp
2pd_12_2b	3	50.27	3.70	0.26	18.53	0.33	12.11	11.10	0.59	0.04	0.00	96.97	amp
2pd_12_3	1	67.37	21.43	0.00	0.07	0.01	0.01	2.49	10.45	0.05	0.00	101.87	plag
2pd_12_3	2	52.64	2.36	0.77	9.88	0.08	18.52	11.23	1.20	0.06	0.00	96.82	amp
2pd_12_3	3	49.88	3.82	0.27	20.09	0.31	11.11	11.27	0.64	0.05	0.00	97.49	amp
2pd_17_1	1	64.93	22.33	0.02	0.38	0.00	0.01	3.83	9.27	0.09	0.01	100.87	plag
2pd_17_1	2	36.02	24.62	0.00	6.01	0.06	2.92	20.57	0.02	0.02	0.01	90.26	ep
2pd_17_1	3	36.37	23.93	0.00	5.43	0.09	1.27	21.62	0.03	0.00	0.01	88.74	ep
2pd_17_1	4	67.04	21.76	0.02	0.07	0.03	0.00	2.94	10.22	0.06	0.01	102.15	plag
2pd_17_2	1	37.23	23.77	0.04	9.68	0.00	0.11	22.51	0.02	0.00	0.01	93.37	ep
2pd_17_3	1	52.15	0.59	0.25	8.63	0.22	15.02	19.99	0.51	0.01	0.01	97.39	amp
2pd_17_3	2	66.62	19.13	0.04	0.07	0.00	0.00	0.93	11.12	0.05	0.00	97.97	plag
2pd_17_3	3	51.78	0.00	0.17	9.12	0.25	15.07	19.68	0.57	0.00	0.00	96.65	amp
2pd_17_3	4	67.69	19.45	0.02	0.21	0.02	0.03	1.59	10.54	0.06	0.14	99.76	plag
2pd_17_3	5	52.67	0.27	0.03	7.73	0.23	15.13	21.14	0.52	0.01	0.00	97.74	amp
2pd_17_3	6	52.91	0.00	0.06	7.42	0.22	15.15	21.48	0.48	0.00	0.00	97.72	amp
2pd_17_3	7	69.12	20.48	0.03	0.25	0.00	0.05	1.09	10.81	0.06	0.01	101.91	plag
235 R1 28_3	1	49.35	0.15	0.01	22.45	1.38	3.56	22.65	0.13	0.01	0.01	99.69	amp
235 R1 28_3	2	49.06	0.10	0.01	23.63	1.63	2.23	22.46	0.13	0.00	0.00	99.26	amp
235 R1 28_3	3	50.87	0.52	0.00	16.54	0.96	7.51	23.10	0.22	0.01	0.00	99.72	amp
235 R1 28_3	4	51.09	0.76	0.00	15.73	0.85	8.13	23.29	0.25	0.00	0.00	100.08	amp
235 R1 28_3	5	49.79	1.05	0.00	21.76	0.21	5.29	21.26	0.91	0.00	0.00	100.27	amp
235 R1 28_3	6	50.26	1.09	0.01	18.96	0.19	7.03	21.57	0.93	0.00	0.01	100.04	amp
235 R1 28_3	7	32.57	14.92	0.04	22.49	0.22	18.71	1.31	0.03	0.01	0.01	90.32	chl
235 R1 28_3	8	29.46	16.20	0.03	22.77	0.24	19.42	0.18	0.00	0.00	0.01	88.31	chl
235 R1 28_3	9	29.23	16.20	0.02	23.23	0.24	19.42	0.07	0.00	0.00	0.01	88.42	chl
235 R1 28_3	10	29.71	16.71	0.02	23.49	0.21	18.84	0.17	0.01	0.03	0.00	89.18	chl
R14 JGB_4	1	53.08	1.81	0.29	14.94	0.23	14.98	12.43	0.55	0.02	0.13	98.47	amp
R14 JGB_4	2	64.63	23.07	0.00	0.51	0.00	0.00	4.50	9.14	0.09	0.00	101.94	plag
R14 JGB_4	3	53.15	1.89	0.34	15.08	0.25	15.59	11.08	0.51	0.04	0.09	98.02	amp
R14 JGB_4	4	65.77	22.18	0.01	0.51	0.00	0.00	3.43	9.85	0.07	0.00	101.82	plag
R14 JGB_4	5	50.38	4.24	0.41	15.41	0.21	14.47	11.22	0.97	0.06	0.06	97.42	amp
R14 JGB_4	6	63.95	23.42	0.03	0.29	0.01	0.00	4.74	9.05	0.07	0.00	101.56	plag
R14 JGB_4	7	54.81	28.43	0.05	0.54	0.00	0.03	11.12	5.39	0.06	0.04	100.47	plag
R14 JGB_3	1	55.07	27.93	0.06	0.85	0.00	0.04	10.72	5.54	0.04	0.00	100.25	plag
R14 JGB_3	2	51.40	3.95	0.42	13.94	0.19	15.86	11.39	0.95	0.04	0.10	98.24	amp
R14 JGB_3	3	63.26	23.20	0.05	0.70	0.00	0.01	4.89	9.03	0.09	0.00	101.23	plag
R14 JGB_3	4	49.03	4.77	0.26	16.42	0.21	13.27	11.64	0.99	0.04	0.12	96.76	amp
R14 JGB_3	5	65.38	22.87	0.01	0.29	0.00	0.00	4.07	9.38	0.05	0.00	102.07	plag
R14 JGB_3	6	53.22	28.78	0.09	0.73	0.00	0.03	11.89	4.82	0.02	0.01	99.58	plag
R14 JGB_2	1	55.71	1.59	0.01	12.11	0.36	22.37	6.07	0.32	0.02	0.03	98.60	amp
R14 JGB_2	2	54.41	2.93	0.05	7.09	0.18	21.62	11.41	0.73	0.05	0.03	98.50	amp
R14 JGB_2	3	38.59	16.73	0.43	10.26	0.08	21.83	0.02	0.50	7.03	0.27	95.74	phl

R14 JGB_2	4	53.76	28.27	0.07	0.95	0.01	0.07	11.60	4.98	0.14	0.01	99.85	plag
R14 JGB_2	5	38.26	16.75	0.47	9.49	0.12	22.13	0.06	0.33	6.92	0.21	94.75	phl
R13 J_3	1	37.62	24.73	0.05	11.12	0.09	0.00	23.38	0.01	0.00	0.00	96.99	ep
R13 J_3	2	69.31	19.59	0.01	0.14	0.00	0.00	0.09	11.85	0.01	0.00	101.00	plag
R13 J_1	1	25.78	18.62	0.04	28.20	0.17	14.55	0.10	0.01	0.00	0.01	87.49	chl
R13 J_1	2	25.52	19.54	0.05	33.39	0.41	10.23	0.42	0.02	0.00	0.02	89.60	chl
R13 J_1	3	43.69	21.41	0.01	3.92	0.02	0.00	24.30	0.06	0.01	0.00	93.42	zeo
R11 JGB_1	1	49.71	31.67	0.05	0.60	0.02	0.04	14.76	3.18	0.05	0.03	100.11	plag
R11 JGB_1	2	45.26	9.55	0.23	13.06	0.20	14.58	10.54	2.07	0.13	0.32	95.95	

Phlogopite, zeolite, and magnetite are the three minor minerals identified. Phlogophite is very distinct that it contains a high percentage of potassium compared to any other minerals studied here. Magnetite is also easily recognizable as it does not have a silica component. Zeolite identification was not obvious, but its total is low, meaning that it is a hydrous mineral. The chemical composition was confirmed by comparison with zeolites from a previous work on Hole 1256D (Alt et al., 2010) and further specified to be laumontite, $Ca_4(Al_8Si_{16}O_{48})\cdot 18H_2O$.

Discussion

The compositions of the three main minerals, amphibole, plagioclase, and chlorite, were plotted and compared to a similar work done by Alt et al. (2010). For amphiboles (Figure 8), the composition obtained in this study matched well with that of Alt et al. (2010). The majority of the amphiboles have ~7.5-8 % Si and a $Mg/(Mg+Fe^{2+})$ range of 0.5 to 0.8. This signifies that most amphiboles obtained on Expedition 335 at depth of >1500 mbsf of Hole 1256D are actinolites. There are several Mg-rich hornblende with high Si content as well. Furthermore, a couple of amphiboles showed relatively higher amount of Si (> 8) not seen by Alt et al. (2010). For both actinolites and hornblendes, chlorine content is low. Following Vanko (1986), this suggests the presence of seawater-like solutions at the time of formation.

Similarly, the analyses of plagioclase and chlorite compositions were compared to Alt et al. (2010) (Figure 9). Most plagioclase showed very low MgO and relatively low anorthite percentages. From this, it can be inferred that most plagioclase analyzed here are secondary

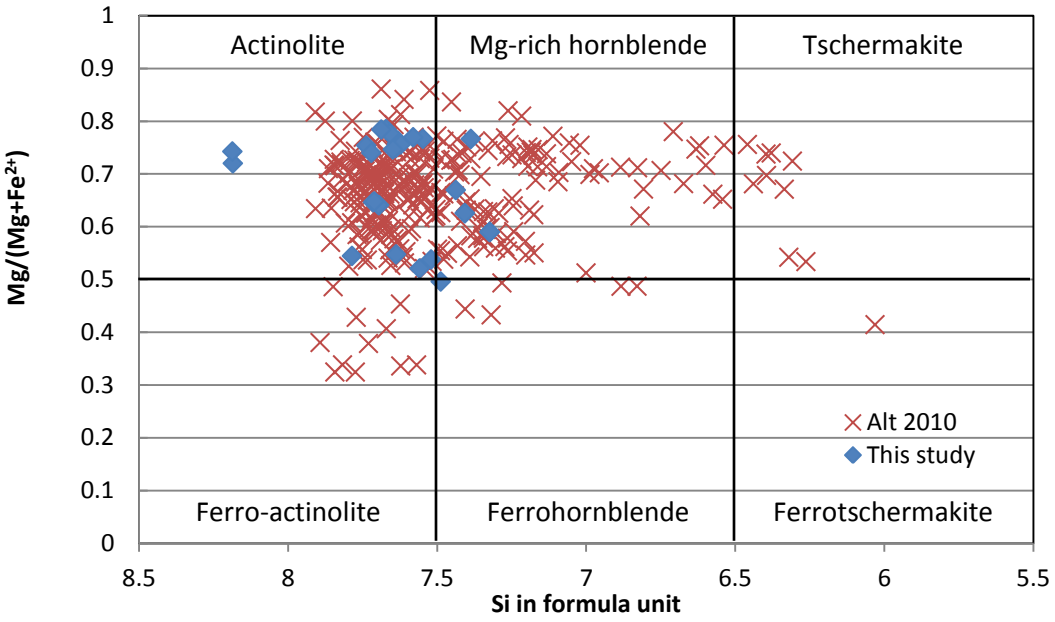

Figure 8. The composition of amphiboles. Amphibole data from Alt et al., 2010 and this study are shown as cross and diamond icons, respectively. Specific minerals within the amphibole group are identified into actinolite, ferro-actinolite, Mg-rich hornblende, ferrohornblende, tschermakite, and ferrotschermakte following Alt et al., 2010.

plagioclase that is replacing igneous plagioclase. A few plagioclase analyses showed higher anorthite percentages, close to 55%. These are likely to be from glanoblastic dikes. Chlorites also followed closely the composition from Alt et al. (2010). They are on the relatively low side in terms of Si content and have mid- Fe/(Fe+Mg) values.

Temperatures at the time of crystallization were calculated and are summarized in Table 2. Eleven useful pairs of amphibole and plagioclase were selected, and then gave a temperature range and average of 425 °C to 663 °C and 550.3 °C, respectively This temperature range is low, in comparison to temperatures estimated for magmatic amphiboles by Coogan et al. (2001), and

implies that there was a hydrothermal influence at the time of the formation of these amphiboles. Typically, magmatic amphiboles yield a temperature of around 800 °C and above whereas cooler temperatures result from hydrothermal crystallization, although temperatures can nevertheless be

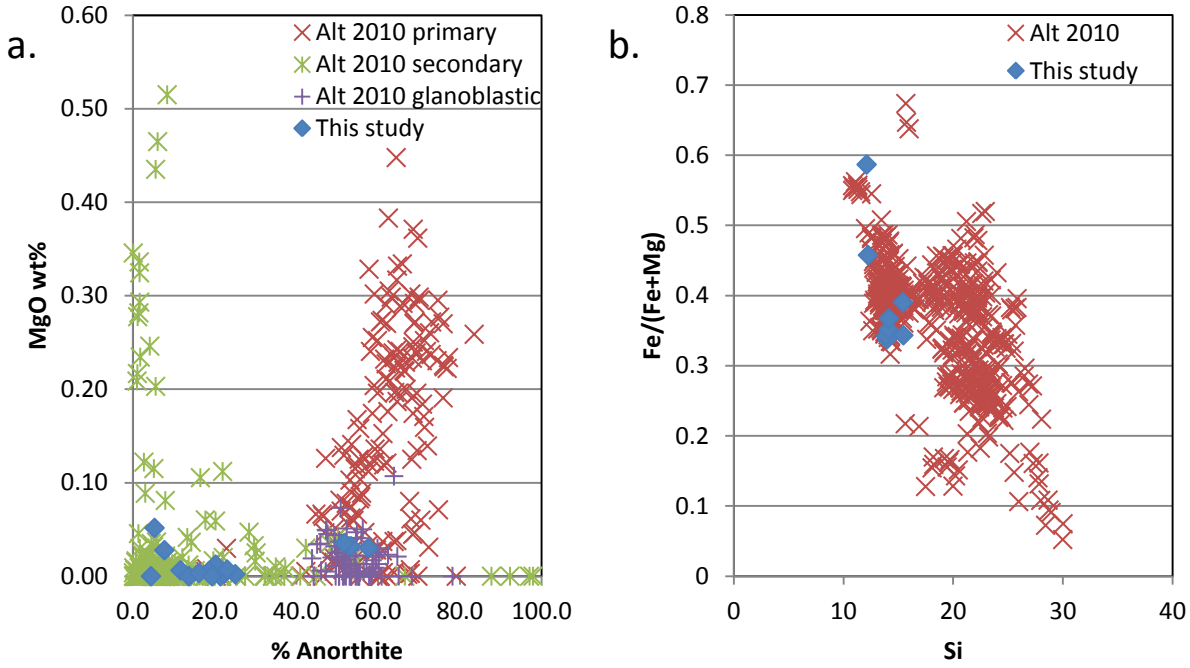

Figure 9. a. Composition of plagioclase. Percent MgO plotted against anorthite percentage (same as Ca percentage). Plagioclase from Alt et al., 2010 is classified into primary, secondary, and glanoblastic plagioclase. Analysis from this study is shown in solid diamonds. b. Composition of chlorites. This study and Alt et al., 2010 are shown in solid diamonds and crosses, respectively.

up to around 700°C for hydrothermal amphiboles (Gillis, 1995; Coogan et al., 2001). Figure 10 illustrates the temperature zone of the minerals studied here in comparison to the overall view of mineral-temperature relationship in Hole 1256D in which temperatures were calculated by various methods by Alt et al. (2010). Figure 11 shows the microprobe images of sample areas where these analyses were completed.

Table 2. Crystallization temperatures calculated from the amphibole-plagioclase equilibrium thermometer. Only pairs of amphiboles and plagioclase in contact were selected and used.

Sample	Amphibole	Plagioclase	T
	Point	Point	° C
2pd_12	1	3	573.87
2pd_12	7	9	502.52
2pd_12	10	9	500.85
2pd_12_3	3	1	461.23
R14 JGB_4	3	4	425.19
R14 JGB_4	5	6	557.68
R14 JGB_4	5	7	663.81
R14 JGB_3	2	1	629.75
R14 JGB_3	4	3	547.23
R14 JGB_3	4	5	532.95
R14 JGB_3	4	6	659.69

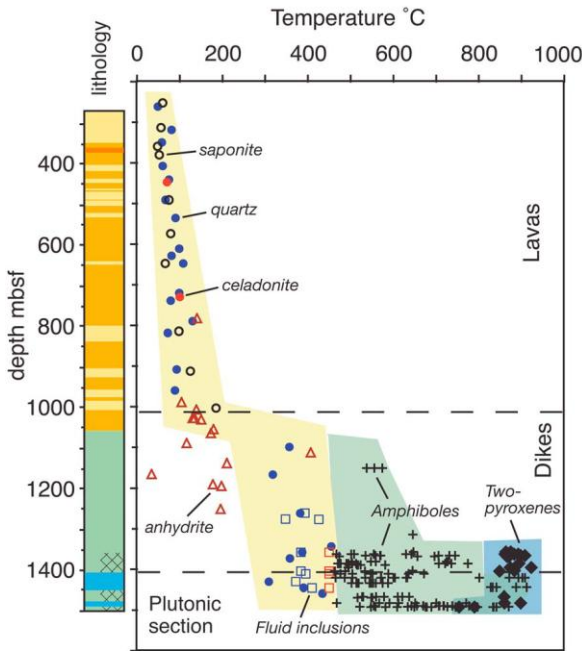

Figure 10. Temperatures obtained from various mineral thermometers by Alt et al., 2010. Amphiboles show a temperature range from mid 400 ℃ to approximately 900 ℃ with average within the range of 550-650 ℃. Temperatures in this study generally agree, although no values above 700 ℃ were obtained.

From the above analyses, it can be inferred that at a depth of 1500 mbsf, hydrothermal fluids are still penetrating. Although this implies that the answer to the ultimate objective of finding the boundary layer and the melt lens is not obtained, it still provides more information about hydrothermal fluids that they are seeping into great depths. In fact, the cooling history of the hydrothermal system at this site is being illustrated here. First, hornblendes formed at high-temperature conditions, then actinolites formed once the temperature started to decrease. Chlorites and epidotes also formed as the temperature decreased even more. Finally, zeolites manifest the lowest temperature phase.

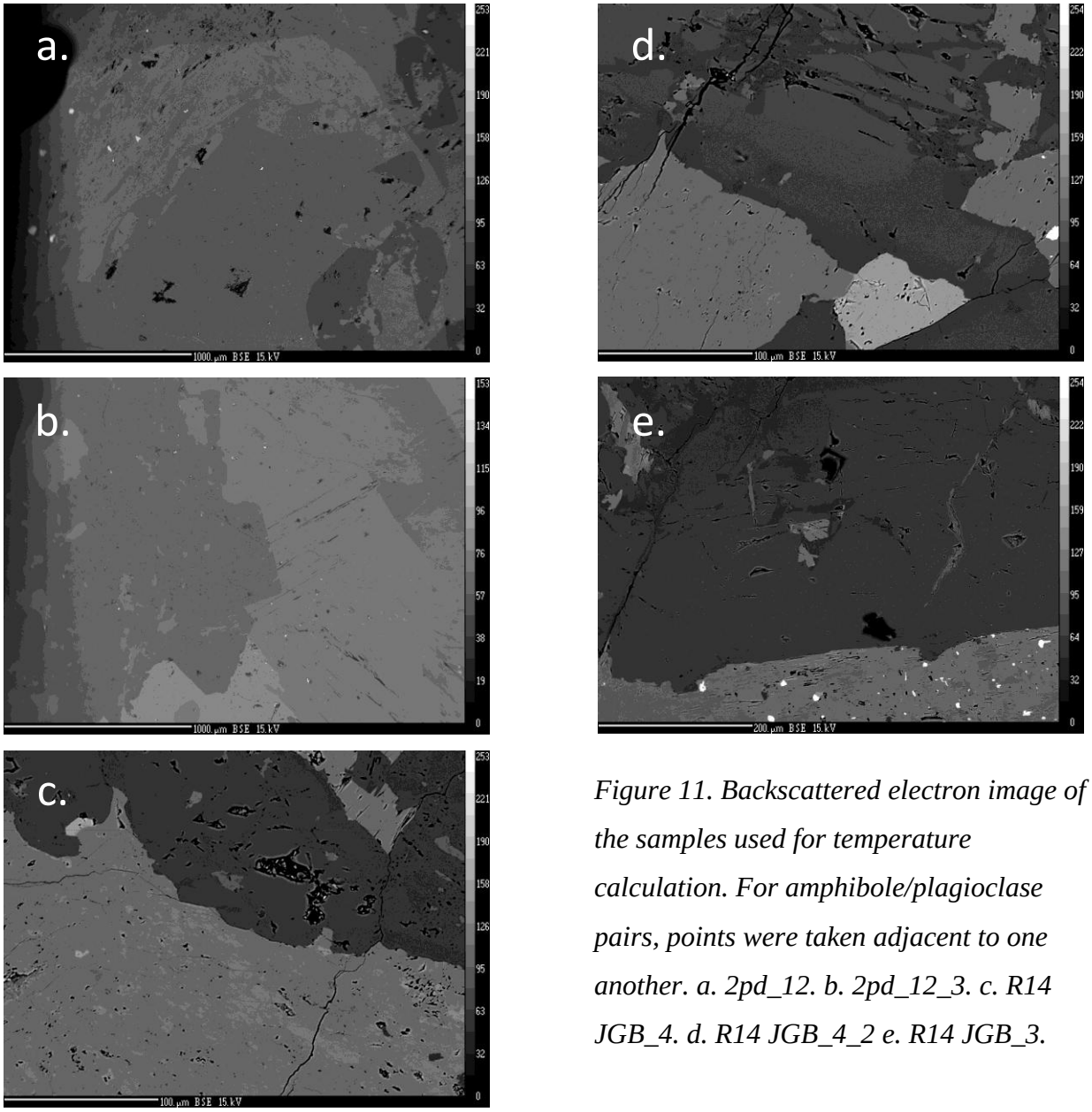

Figure 11. Backscattered electron image of the samples used for temperature calculation. For amphibole/plagioclase pairs, points were taken adjacent to one another. a. 2pd_12. b. 2pd_12_3. c. R14 JGB_4. d. R14 JGB_4_2 e. R14 JGB_3.

Following the model proposed in Alt et al. (2010), the structure and evolution of the hydrothermal system at Hole 1256D is as follows (Figure 12). First, a conductive boundary layer separates a deep axial magma chamber from the dike section. In the dike section, fluids are circulating, but they do not reach below the boundary layer. At this stage, the upper dike section is dominated by circulation of cooler seawater while the lower section contains generally upwelling hydrothermal fluids. There are two major steps in temperature gradients, one between

this lower dike section containing higher temperature hydrothermal fluids and the upper volcanic section containing cooler seawater. The other step occurs at the conductive boundary layer where

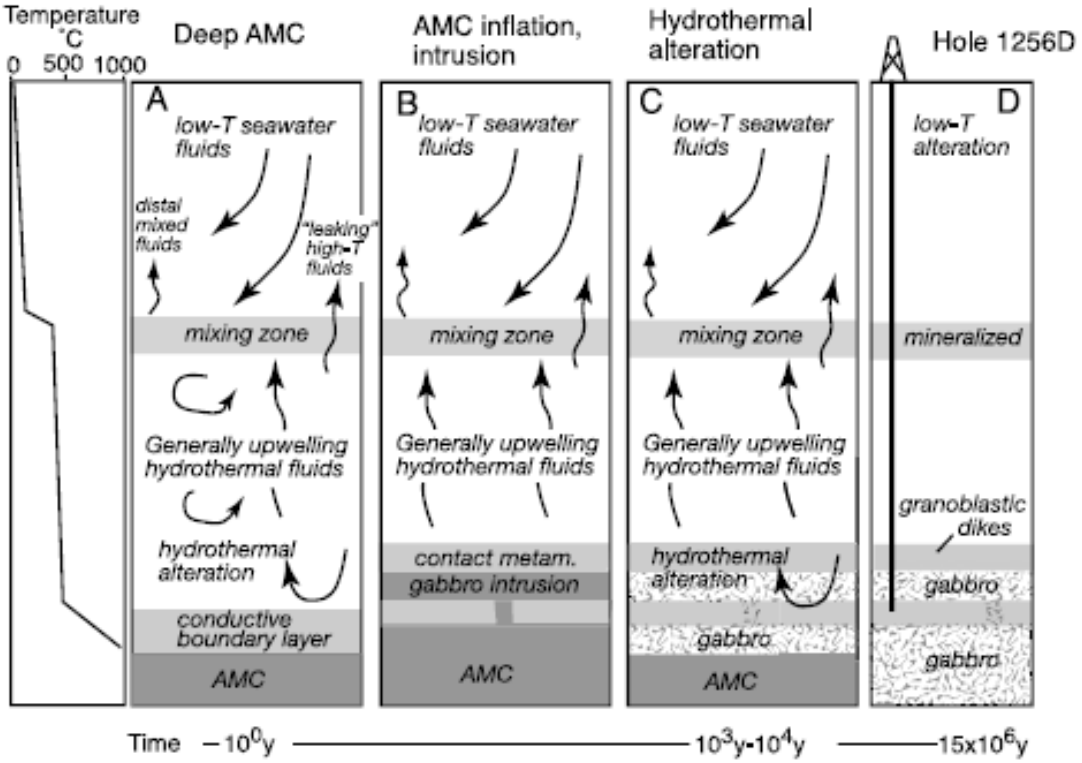

Figure 12. Structure and evolution of alteration processes at Site 1256D proposed by Alt et al. (2010). a. Early stage of hydrothermal alteration. b. Gabbroic intrusion. c. Later stage of hydrothermal alteration. d. Present day structure of the site with Hole 1256D showing its penetration. Temperature gradient shown on the left.

the composition changes from hydrothermally to magmatically dominated. Then, there was a gabbroic intrusion in which the axial magma chamber upwelled into the lower dikes. Here, contact metamorphism took place and the lower dike section saw significant changes where the upper section was relatively unchanged. Eventually the gabbros cooled and crystallized over time. Hydrothermal fluids started to penetrate into the gabbros, altering them hydrothermally. As this site moved away from the axial magma chamber and the East Pacific Rise, the heat source was taken away and hydrothermal activities ceased. The gabbros, dikes, alteration remnants, and

other features that indicate past geological activities at this site were preserved and recovered by the four expeditions that drilled Hole 1256D. Particularly, this study focuses on the temperature and composition of granoblastic dikes and gabbros during the later stage of hydrothermal alteration after the intrusion of gabbros (Figure 12c). The lowest point of Hole 1256D in Figure 12d corresponds to the samples recovered by Expedition 335, which were analyzed here. As the figure illustrates, this is a crucial zone to understand as hydrothermal fluids were just beginning to penetrate into the gabbros. Again, it is recognizable that a few meters more of successful drilling will deepen the hole into the larger gabbroic section which is believed to be the remnants of the heat source, the axial magma chamber.

Conclusions

Hydrothermal systems play a major role in the oceans through various processes. Our knowledge about them is expanding, and it is crucial to understand more about these mysterious phenomenon hidden deep undersea. IODP has contributed a lot in this process, and particularly Hole 1256D drilled by one ODP and three IODP expeditions provides valuable information concerning the deep hydrothermal alteration, near the border of magmatic heat source and the overlying crust. The objective of the last expedition, Expedition 335, was to deepen the hole into the gabbroic section where it is believed to be the remnant of the magma chamber. The project fell short of achieving this objective, however still recovered useful samples at depths of >1500 mbsf. This study analyzed the granoblastic dike and gabbro samples recovered from Expedition 335 to give further information about the composition and temperature at a critical section of the hole.

The analysis in this study used a microprobe analyzer to obtain the chemical composition of the minerals. Each mineral was identified according to the chemical composition and further

analyzed according to the percentages of certain elements in amphiboles, plagioclase, and chlorites. The edenite-richterite thermometer was used to calculate the temperature of amphibole/plagioclase at the time of their crystallization. This resulted in a range of 425 °C to 663 °C, being consistent with temperature analyses done by other authors on samples recovered by previous expeditions.

This study gives further insight into the subsurface structure at Site 1256D and the general overview of hydrothermal systems at fast spreading centers such as the East Pacific Rise. We also analyze the limits of current data and encourage deepening of the hole. In a few meters, Hole 1256D will likely penetrate into the gabbroic section. Information that becomes available from this section will very likely provide useful knowledge to better understand the structure and evolution of hydrothermally altered oceanic subsurface. When this happens, geochemical and petrological analyses such as those used in this study will be one method to provide meaningful results. Additionally, rare earth element (REE) and isotopic analyses of amphiboles will be beneficial; for this study, the next task is to reevaluate the outcomes using REE and isotopic analyses. In all, our next objective is to deepen Hole 1256D, analyze recovered samples, and reestablish a more thorough model of hydrothermally altered oceanic crusts.

References

Alt, J. C., C. Laverne, R. M. Coggon, D. A. H. Teagle, N. R. Banerjee, S. Morgan, C. E. Smith‐Duque, M. Harris, and L. Galli, Subsurface structure of a submarine hydrothermal system in ocean crust formed at the East Pacific Rise, ODP/IODP Site 1256, *Geochem. Geophys. Geosyst*., 11, 2010.

Alt, J. C., Subseafloor Processes in Mid-Ocean Ridge Hydrothermal Systems, *Geophys. Monograph, 91*, 1995.

Anderson, R.N. and M.A. Hobart, The relationship between heat flow, sediment thickness and age in the Eastern Pacific, *J. Geophys. Res., 81*, 2968-2969, 1976.

Casey, J.F., J.F. Dewey, P.J. Fox, J.A. Karson, and E. Rosencrantz, Heterogeneous nature of oceanic crust and upper mantle: a perspective from the Bay of Islands Ophiolite Complex, In: *The Sea, v.* 7, *The Oceanic Lithosphere,* edited by C.E. Emiliani, pp. 305-338, J. Wiley, New York, 1981.

Coleman, R.G., *Ophiolites-Ancient oceanic lithosphere?,* 229 pp., Springer-Verlag, 1977.

Coogan, L. A., R. N. Wilson, K. M. Gillis, and C. J. Macleod, Near‐solidus evolution of oceanic gabbros: Insights from amphibole geochemistry, *Geochim. Cosmochim. Acta, 65(23)*, 4339‐4357, 2001

Detrick, R.S., P. Buhl, E. Vera, J. Mutter, J. Orcutt, J. Madsen, and T. Brocher, Multichannel seismic imaging of a crustal magma chamber along the East Pacific Rise, *Nature, 326,* 35- 41, 1987.

Edmond, J. M., C. Measures, R. E. McDuff, L. H. Chan, R. Collier, B. Grant, L. I. Gordon, and J. B. Corliss, Ridge crest hydrothermal activity and the balances of the major and mnor elements in the ocean: Galapagos data, *Earth. Planet. Sci. Lett. 46*, 1-18, 1979a.

Expedition 335 Scientists, 2011. Superfast spreading rate crust 4: drilling gabbro in intact ocean crust formed at a superfast spreading rate. IODP Prel. Rept., 335. doi:10.2204/iodp.pr.335.2011

Fehn, U., K.E. Green, R.P. Von Herzen, and L.M. Cathles, Numerical models for the hydrothermal field at the Galapagos Spreading Center, *J. Geophys. Res., 88,* 1033-1048, 1983.

France, L., B. Ildefonse, and J. Koepke, Interactions between magma and hydrothermal system in Oman ophiolite and in IODP Hole 1256D: Fossilization of a dynamic melt lens at fast spreading ridges, *Geochem. Geophys. Geosyst., 10,* Q10O19, 2009b.

Gillis, K. M., Controls on hydrothermal alteration in a section of fast‐spreading oceanic crust, *Earth Planet. Sci. Lett., 134,* 473‐489, 1995.

Harding, A.J., J. Orcutt, M. Kappus, E. Vera, J. Mutter, P. Buhl, R. Detrick, and T. Brocher, The structure of young oceanic crust at 13 ·N on the East Pacific Rise from expanding spread profiles, *J. Geophys, Res., 94,* 12,163-12,196, 1989.

Harper, G.D., The Josephine ophiolite, northwestern California, *Geol. Soc. Am. Bull., 95,* 1009-1026, 1984.

Holland TJB, Powell R, Plagiodase feldspars: activity-composition relations based upon Darken's Quadratic Formalism and Landau theory. *Am Mineral 77*:53 61. 1992.

Holland, T. J. B., and J. Blundy, Non‐ideal interactions in calcic amphiboles and their bearing on amphibole‐plagioclase thermometry, *Contrib. Mineral. Petrol., 116,* 433‐447, 1994.

Kent, G.M., A.J. Harding, and J.A. Orcutt, Evidence for a smaller magma chamber beneath the East Pacific Rise at 9·30'N, *Nature, 344,* 650-653, 1990.

Koepke, J., D. M. Christie, W. Dziony, F. Holtz, D. Lattard, J. Maclennan, S. Park, B. Scheibner, T. Yamasaki, and S. Yamasaki, Petrography of the dike‐gabbro transition at IODP Site 1256 (equatorial Pacific): The evolution of the granoblastic dikes, *Geochem. Geophys. Geosyst., 9*, Q07O09, 2008.

Koepke, J., L. France, T. Müller, F. Faure, N. Goetze, W. Dziony, and B. Ildefonse, Gabbros from IODP Site 1256, equatorial Pacific: Insight into axial magma chamber processes at fast spreading ocean ridges, *Geochem. Geophys. Geosyst., 12*, Q09014, 2011.

Lister, C.R.B., "Active" and "passive" hydrothermal systems in the ocean crust. Predicted physical conditions. in *The dynamic environment of the ocean floor,* edited by K.A. Fanning and F.T. Manheim, pp. 441-470, D.C. Heath, Lexington, MA, 1982.

Lister, C.R.B., On the thermal balance of a mid-ocean ridge, Geophys. 1. R. Astr. Soc., 26,515-535, 1972.

McClain, J.S., J.A. Orcutt, and M. Burnett, The East Pacific Rise in cross-section: A seismic model, *J. Geophys. Res., 90,* 8627- 8640, 1985.

Moores, E.M., and F.J. Vine, The Troodos Massif, Cyprus and other ophiolites and oceanic crust: evaluations and implications, *Roy. Soc. London, Phil. Trans., A268,* 443-466, 1971.

Morton, J.L. and N.H. Sleep, A mid-ocean ridge thermal model: constraints on the volume of axial hydrothermal heat flux, *J. Geophys. Res., 90,* 11,345-11,353, 1985.

Mottl, M.J. and C.G. Wheat, Hydrothermal circulation through mid-ocean ridge flanks: fluxes of heat and magnesium, *Geochim. Cosmochim. Acta, 58,* 2225-2237, 1994.

Nicolas, A., *Structures of ophiolites and dynamics of oceanic lithosphere,* 367 pp., Kluwer Academic, Dordrecht, 1989.

Perfit, M. R., D. A. Gust, A. E. Bence, R. J. Arculus, and S. R. Taylor, Chemical characteriscs of island-arc basalts: Implications for mantles sources, *Chem. Geol., 30,* 227-256, 1980.

Pezard, P. A., Electrical properties of mid-ocean ridge basalt and implications for the structure of the upper oceanic crust in Hole 504B, *J. Geophys. Res. 95, 9237-9266,* 1990.

Sclater, J. G., B. parsons, and C. Jaupart, Oceans and continents: similarities and differences in the mechanisms of heat loss, *J. Geophys. Res., 86,* 11, 522-11535, 1981.

Sinton, J.M., and R.S. Detrick, Mid-ocean ridge magma chambers, *J. Geophys. Res., 97,* 197-216, 1992.

Stein, C. A., and S. Stein, Constraints on hydrothermal heat flux through the oceanic lithosphere from global heat flow, *J. Geophys. Res., 99,* 3081-3096, 1994.

Teagle, D. A. H., and Expedition 309/312 Scientists, Superfast Spreading Rate Crust 2 and 3 [online], *Proc. Integrated Ocean Drill. Program,* 309/312. 2006. (Available at http://iodp.tamu.edu/publications/exp309_312/30912toc.htm)

Thompson, G., Basalt-seawater interaction, in *Hydrothermal processes at seafloor spreading centers*, edited by P. A. Rona, K. Bostrom, and K. L. Smith, pp. 225-278, Plenum, New York, 1983.

Tominaga, M., D. A. H. Teagle, J. C. Alt, and S. Umino, Determination of the volcanostratigraphy of oceanic crust formed at superfast spreading ridge: Electrofacies analyses of ODP/IODP Hole 1256D, Geochem. Geophys. Geosyst., 10, Q01003, 2009. doi:10.1029/2008GC002143.

Toomey, D.R., G.M. Purdy, S. Solomon, and W. Wilcox, The three dimensional seismic velocity structure of the East Pacific Rise near latitude 9o30'N, *Nature, 347,* 639-644, 1990.

Vanko, D. A., High-chlorine amphiboles form oceanic rocks: product of highly-saline hydrothermal fluids?, *Am. Mineral. 71.* 51-59, 1986.

Vera, E.E., P. Buhl, J.C. Mutter, A.J. Harding, J.A. Orcutt, and R.S. Detrick, The structure of 0-0.2 My old oceanic crust at 9°N in the East Pacific Rise from expanded spread profiles, *J. Geophys. Res., 95,* 15,529-15,556, 1990.

Williams, D.L., R.P. Von Herzen, J.G. Sclater, and R.N. Anderson, The Galapagos Spreading Center: Lithospheric cooling and hydrothermal circulation, *Geophys. J.R. Astr. Soc., 38,* 587-608, 1974.

Wilson, D. S., et al., Drilling to gabbro in intact ocean crust, *Science*, 312, 1016–1020, 2006. doi:10.1126/science.1126090.

Zinder, A., and S. R. Hart, Chemical geodynamics, *Ann. Rev. Earth. Planet. Sci., 14*, 115-118, 1986.